AIAA JOURNAL
Vol. 33, No. 10, October 1995

Computational Study of Large-Disturbance Oscillations in Unsteady Supersonic Combustion Around Projectiles

Akiko Matsuo* and Kozo Fujii†
Institute of Space and Astronautical Science, Sagamihara 229, Japan

Unsteady combustion around a spherical projectile in supersonic flows is numerically studied using the simplified two-step chemical reaction model consisting of the induction and the exothermic reactions. A series of simulations indicates that the intensity of the concentration of the heat release is a key parameter to determine the regime of the unsteady flowfield. Flow features of the unsteady combustion with low-frequency and high-amplitude oscillation, which is called the large-disturbance regime, are reproduced when the concentration of the heat release of the chemical reaction is high. Mechanism of the large-disturbance regime is clarified based on the histories of the density and pressure profiles on the stagnation streamline and the flowfield in front of the projectile body. The period and amplitude of the oscillation corresponding to the shock pressure behind the bow shock agree with experimental observations, and the reproduction of the large-disturbance regime in the present simulation is confirmed.

Nomenclature

E_1, E_2 = activation energies
k_1, k_2 = reaction rate constants
Q = exothremic energy per unit gram
ρ = constant density
τ = oscillation period
τ_s = induction time

Introduction

PERIODIC oscillation of shock-induced combustion around a spherical projectile flying at hypervelocity into a combustible gas is observed under a limited condition. The oscillation is categorized into two types of flow regimes, the regular regime and the large-disturbance regime. In the first type, oscillation is very regular. In the second type, oscillation is less regular but much more pronounced than that of the first type; the period of oscillation is also several times longer. Excellent data[1–5] for the study of such supersonic combustion or detonation are provided by the ballistic range experiments performed in the 1960s and 1970s, and visualized images of the flow field around the projectiles were recorded at that time.

In those experiments,[1–5] projectiles were fired into several kinds of premixed gas mixtures, and the effect of the variation of the speed range on the period of oscillation was shown. The oscillation period depends on the projectile speed in both the regular and the large-disturbance regimes and is a function of the induction time behind normal segment of the bow shock. Here, the C–J speed is not directly related to the unsteady phenomenon of the shock-induced combustion. The C–J speed, however, has an important meaning for the existence of the shock-induced combustion supported by the projectile. When the projectile speed is greater than the C–J speed, the detonation wave established by the shock-induced combustion never overtakes the projectile, and the induction time become exponentially shorter so that the oscillations disappear in the flowfield. If the projectile speed is less than the detonation speed, it is possible that the bow shock grows to the self-sustained detonation wave[1] and runs upstream away from the projectile or that the exothermic reaction does not occur behind the bow shock because the gas temperature does not reach the ignition temperature. Therefore, periodic oscillation of shock-induced combustion supported by the projectile is a rare phenomenon and is usually observed when the projectile speed is in the vicinity of C–J speed.

Ruegg and Dorsey[1] investigated the problems of stabilizing combustion and detonation by the observation of a 20-mm spherical projectile fired into a stoichiometric mixture of hydrogen and air. They presented experimental results showing the regular and large-disturbance regimes. The large-disturbance regime was separate and distinct from the regular regime, but they did not attempt to identify the flow features of either regime. Figures 1a and 1b are the experimental output obtained by their work. These figures are typical flow patterns characterizing regular regime $M_\infty = 4.9$, $P = 0.25$ atm (Fig. 1a), and large-disturbance regime, $M_\infty = 4.8$, $P = 0.5$ atm (Fig. 1b).

Alpert and Toong[2] also investigated the same periodic density variations in the burned gas observed in the nose region of hypersonic blunt body flows by means of ballistic range experiments and a one-dimensional wave interaction analysis. Two regimes of unsteady flow were found in their works when 12.7-mm-diam spherical or flat-nosed projectiles were fired into lean hydrogen-oxygen diluent mixtures. When there is no dilution of the one-quarter stoichiometric hydrogen-oxygen mixture at an initial pressure of 200 torr, the large-disturbance flow regime is usually observed. They have proposed a one-dimensional model to explain the periodicity of the large-disturbance regime. Their mechanism explains that one period of the large-disturbance regime is the long series of wave interactions of summing cycles of four wave interactions of the regular regime. Each wave interaction depends on the strength of the reaction shock, so that small changes in the degree of attenuation of reaction shocks sensitively occur.

Abouseif and Toong[6] investigated the phenomenon of one-dimensional piston-supported gaseous detonations numerically and analytically. In their numerical calculations, a one-step, first-order, irreversible reaction obeying an Arrhenius rate expression was

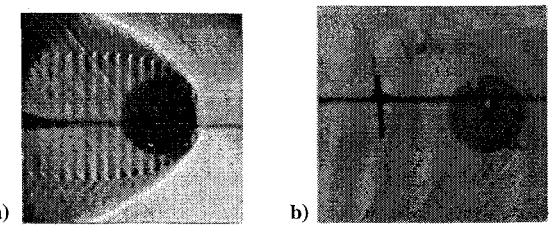

Fig. 1 Experimental output by Ruegg and Dorsey[1]: a) regular regime, $M_\infty = 4.9$, $P = 0.25$ atm and b) large-disturbance regime, $M_\infty = 4.8$, $P = 0.5$ atm.

Presented as Paper 94-0764 at the AIAA 32nd Aerospace Sciences Meeting, Reno, NV, Jan. 10–13, 1994; received Jan. 28, 1994; revision received March 27, 1995; accepted for publication April 4, 1995.

*Research Fellow of the Japan Society for the Promotion of Science; currently Research Associate, Department of Mechanical Engineering, Keio University, Japan. Member AIAA.

†Associate Professor, High-Speed Aerodynamics Division. Member AIAA.

employed. An approximate linearized stability theory was developed for the case of a high-activation-energy reaction, and the mechanism of instability was identified. The theory predicted the period of the low- (large-disturbance regime) and the high-frequency (regular regime) instability modes observed in the blunt body flow experiments by Alpert and Toong.[2]

The experimental works[1–5] also indicate the effect of the projectile scale. A 9 mm diam is used in the experiment of Behrens[4] et al., and the gas pressure is 0.55 atm in H_2/air. The flowfields show the regular regime unsteady combustion in the various speed ranges. On the other hand, Ruegg and Dorsey[1] use a 20-mm-diam projectile and 0.5 atm gas pressure in H_2/air. The large-disturbance regime unsteady combustion appears in the experimental results. The behavior of the chemical reaction process behind the normal segment of the bow shock, is almost the same in both the cases, but the smaller projectile case shows the regular regime and larger projectile case shows the large-disturbance regime. The reason considered for the difference is that the change of the projectile scale implicitly affects the ratio of the fluid scale to the reaction scale.

Even with the experimental and analytical studies, the detailed mechanism of the large-disturbance regime have not been clarified, and the mechanism proposed by Alpert and Toong[2] has not been proved so far. In the present study, the mechanism of the large-disturbance regime is qualitatively discussed based on time-sequential data of the flowfield obtained by numerical simulations, and a new model for the large-disturbance regime is proposed.

Mechanism of Unsteadiness

Regular Regime

In this section, the mechanism of the regular regime is briefly described for use in the future comparative discussion on the large-disturbance regime. A model of the mechanism of the periodic density unsteadiness, the so-called regular regime, was proposed by McVey and Toong[3] using an x–t diagram between the bow shock and reaction front on the stagnation streamline based on the experimental observations and a one-dimensional wave interaction theory.

In recent years, with the progress of computers, several researchers have carried out numerical simulations of such flowfields. Throughout these simulations, the model proposed by McVey and Toong was proved to be correct, and at the same time, more details of the physical phenomenon were revealed. Matsuo and Fujiwara[7,8] and Matsuo et al.[9] proposed an improved flow mechanism model, which is shown in Fig. 2. From the new reaction region, a compression wave, the so-called reaction shock, moves upstream to the bow shock, and the another moves in the opposite direction to the projectile body. The former wave and the latter wave interact with

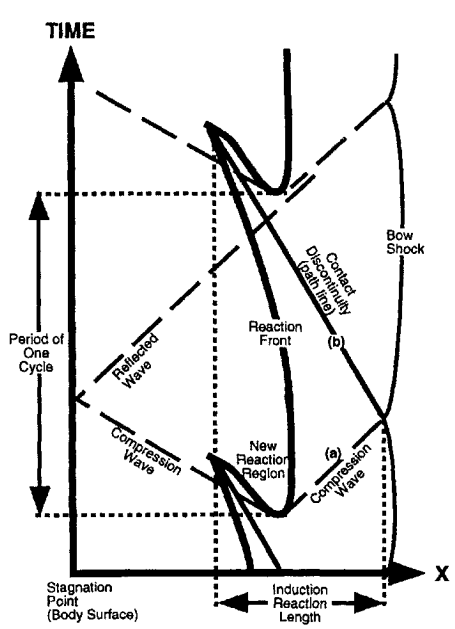

Fig. 2 Wave interaction model x–t diagram of the regular regime proposed by Refs. 7–9.

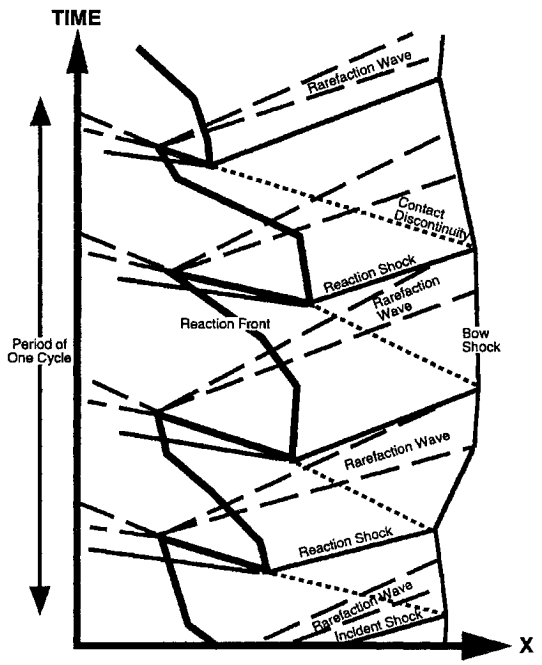

Fig. 3 Wave interaction model x–t diagram of the large-disturbance regime proposed by Alpert and Toong.[2]

the bow shock and generate a contact discontinuity. In general, the gas temperature behind the contact discontinuity is higher than that in front of it. The higher temperature gas has a shorter induction time, although the fluid velocity across the contact discontinuity is the same. The gas behind the contact discontinuity begins to react before the contact discontinuity reaches the original reaction front. This mechanism is like a one-dimensional shock-tube problem. The one cycle corresponds to the period of the compression wave and the contact discontinuity traveling within the induction length between the bow shock and the reaction front into the unburned gas. The period of oscillation obtained by numerical investigation[9] is

$$\tau/\tau_s \approx 1.38$$

The compression waves propagating toward the stagnation point are not negligible for the generalized model.

Large-Disturbance Regime

Alpert and Toong[2] have proposed a mechanism for the large-disturbance regime. The mechanism takes into account the strength of the reaction shocks during the wave interactions and is shown in Fig. 3 as an x–t diagram of wave interactions. It is nearly identical to that in Fig. 2 with the following exception: rarefactions do not overtake and attenuate reaction shocks during any cycle. The x–t diagram in Fig. 3 represents one possible wave interaction. An incident shock, which is reaction shock released at the reaction front, interacts with the bow shock at the beginning point of one cycle. The incident shock is not overtaken and attenuated by a following rarefaction. Then, the distance between the points of formation and extinguishment of the reaction front becomes longer compared with the total length of the induction zone. The period of the one cycle of the large-disturbance regime will be much larger than that of the wave-interaction cycle of Fig. 2 since only one reaction shock reaches the bow shock during the complete cycle of the regular regime. The total period of the long series of wave interactions in the large-disturbance regime is obtained by summing the time intervals required for each formation and the time intervals required for each rightward facing reaction shock to reach the bow shock. Moreover, it should be noted that small changes in the degree of attenuation of reaction shocks during the wave interaction process in Fig. 3 could cause cycle to cycle variations in the period. They found that the period of oscillation based on the proposed mechanism was given for the low-frequency mode (large-disturbance regime),

$$3.8 < \tau/\tau_s < 5.4$$

On the other hand, the experimental results (Fig. 6 in Ref. 2) suggested that the period of oscillation of the large-disturbance regime around the spherical projectiles into an H_2/air mixture is

$$3 < \tau/\tau_s < 12$$

and the average value derived by the method of least squares is

$$\tau/\tau_s \approx 5.23$$

The mechanism proposed by Alpert and Toong[2] would be appropriate to describe the large-disturbance regime oscillation for the period of oscillation.

Zero-Dimensional Analysis

The zero-dimensional analysis, which is a time-integration of the species equations in zero dimension in space under the constant volume mode (total density ρ is constant) of the thermally perfect gas mixture, is carried out in this section to understanding the characteristics of the chemical reaction progress behind the normal segment of the bow shock:

$$\frac{\partial \rho_i}{\partial t} = \omega_i \tag{1}$$

The hydrogen–oxygen reaction mechanism[11,15] consisting of 9 species and 19 reactions in Table 1 is used. This procedure was used in previous work[9] to understand the phenomena of the periodicity for the regular regime. The experimental conditions for Figs. 1 are used. As an initial condition, all of the values are given by the Rankin–Hugoniot relation for the projectile speed under the thermally perfect gas. The temperature profiles in Figs. 4a and 4b correspond to the Ruegg and Dorsey experiment in Fig. 1. The Fig. 4a profile is under the same conditions as Fig. 1a, the regular regime, $M_\infty = 4.9$, $P = 0.25$ atm, and $T = 300$ K, and the Fig. 4b profile is under the conditions of Fig. 1b, the large-disturbance regime, $M_\infty = 4.8$, $P = 0.5$ atm, and $T = 300$ K. The two profiles in Fig. 4 show the difference in the temperature increase. In the Fig. 4a and 4b profiles, the induction times are about 1.17 and 0.74 μs and the periods of the temperature increase are 2.73 and 1.23 μs, respectively. Here, the induction time is defined as the time required for 10% of the total temperature rise. The period of the temperature increase is defined as the time required to increase the temperature up to 95% of the total temperature after the induction time.

Based on the idea that explained the mechanism of the regular regime, the Fig. 4b case should show higher frequency because the induction time is shorter. The frequency, however, is lower than the Fig. 4a case, and the amplitude of density oscillation is much higher than the regular regime unsteady combustion. This indicates that the large-disturbance regime unsteady combustion contains a different

Table 1 H_2–O_2 reaction mechanism,[15] $k_{f_k} = AT^{n_k} \exp(-E_k/RT)$

k, s	Reaction, mole	A, cm^3	n, cal	E, K
1	$H_2 + O_2 = HO_2 + H$	1.00×10^{14}	0	56,000
2	$H + O_2 = OH + O$	2.60×10^{14}	0	16,800
3	$O + H_2 = OH + H$	1.80×10^{10}	1	8,900
4	$OH + H_2 = H + H_2O$	2.20×10^{13}	0	5,150
5	$OH + OH = O + H_2O$	6.30×10^{12}	−2	1,090
6	$H + OH + M = H_2O + M$	2.20×10^{22}	−1	0
7	$H + H + M = H_2 + M$	6.40×10^{17}	−0.6	0
8	$H + O + M = OH + M$	6.00×10^{16}	0	0
9	$H + O_2 + M = HO_2 + M$	2.10×10^{15}	0	−1,000
10	$O + O + M = O_2 + M$	6.00×10^{13}	0	−1,800
11	$HO_2 + H = OH + OH$	1.40×10^{14}	0	1,080
12	$HO_2 + H = H_2O + O$	1.00×10^{13}	0	1,080
13	$HO_2 + O = O_2 + OH$	1.50×10^{13}	0	950
14	$HO_2 + OH = H_2O + O_2$	8.00×10^{12}	0	0
15	$HO_2 + HO_2 = H_2O_2 + O_2$	2.00×10^{12}	0	0
16	$H + H_2O_2 = H_2 + HO_2$	1.40×10^{12}	0	3,600
17	$O + H_2O_2 = OH + HO_2$	1.40×10^{13}	0	6,400
18	$OH + H_2O_2 = H_2O + HO_2$	6.10×10^{12}	0	1,430
19	$H_2O_2 + M = OH + OH + M$	1.20×10^{17}	0	45,500

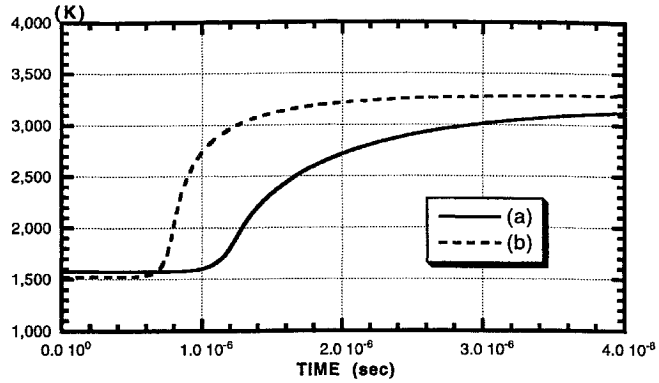

Fig. 4 Temperature profiles by the time-integration procedure in zero dimension in space under the constant volume mode: a) regular regime, $M_\infty = 4.9$, $P = 0.25$ atm, $T = 300$ K and b) large-disturbance regime, $M_\infty = 4.8$, $P = 0.5$ atm, $T = 300$ K.

mechanism for the periodicity and wave interaction. Also, a series of simulations by Matsuo et al.[9] have concluded that the concentration of the heat release with respect to the projectile length or the shock standoff distance is an important factor for the unsteadiness itself because the lower concentration of the heat release did not generate the unsteady flowfield. Here, the characteristic of Fig. 4b is higher concentration of heat release than Fig. 4a, and it is predicted that the higher concentration case might cause the large-disturbance regime in the flowfield.

Here, the term concentration of heat release means the ratio of the reaction period, which is the length or time for the temperature increase, to the shock standoff distance. It does not mean heat release rate.

Simulations of Axisymmetric Flowfield

Based on the zero-dimensional analysis, higher concentration of heat release may be one of the important factors of the large-disturbance regime. Therefore, a parametric study changing the intensity of concentration of heat release is carried out.

Numerical Approach

In the present simulations, the computational domain is limited to the region in front of the hemispherical blunt body, as is shown in Fig. 5. The grid spacings in both the ξ and η directions are equal. Nonreacting flow is solved first, and it is used as an initial condition of the reacting flow simulations. The final grid distribution is created by changing the grid system to adapt the location of the bow shock wave during the computations for nonreacting flow, in order to reduce the grid spacing behind the bow shock wave. The axisymmetric Euler equations are solved by a finite difference method, and unsteady solutions are obtained using the time marching procedure. A second order in time and second order in space explicit difference schemes based on the non-MUSCL total variation diminishing (TVD) approach developed by Yee[16] is used.

Simplified Two-Step Chemical Reaction Model

In the present computations, the following set of model reactions are considered, rather than handling a realistic chemical system undergoing a number of elementary reactions. The simplified mechanism is useful to understand the basic physics of the flowfield because the phenomena can be treated excluding other factors. It has been proved that the following model is useful for the simulation of detonation in the premixed gas in previous work.[7,8,14] Assumptions that were utilized are as follows:

1) The gas is perfect with an adiabatic index $\gamma = 1.4$, generating a constant exothermicity.

2) The gas is nondiffusive, i.e., Euler equations are used.

3) The chemical reaction consists of the following two stages: a) the induction stage where no heat is released, while the progress variable α varies monotonically from 1 to 0 and b) the exothermic reaction stage where heat is released. This stage is triggered at the instant $\alpha = 0$ when the other progress variable β starts decreasing

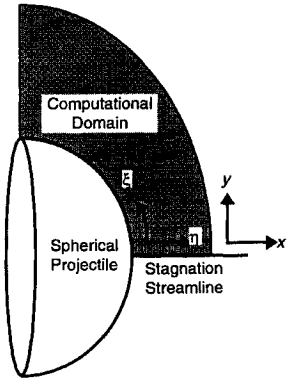

Fig. 5 Computational domain.

from 1 to its equilibrium value $\beta_{eq} > 0$. The amount of heat release is proportional to the change of the progress variable β.

The source terms ω_α and ω_β are expressed as

$$\omega_\alpha \equiv \frac{d\alpha}{dt} = -\frac{1}{\tau_{ind}} = -k_1 \rho \exp\left(-\frac{E_1}{RT}\right) \tag{2}$$

for the induction and for the exothermic reaction,

$$\omega_\beta \equiv \frac{d\beta}{dt} = \begin{cases} = 0, & \alpha > 0 \\ = -k_2 P^2 \left[\beta^2 \exp\left(-\dfrac{E_2}{RT}\right) - (1-\beta)^2 \right. & \\ \left. \times \exp\left(-\dfrac{E_2 + Q}{RT}\right)\right], & \alpha \le 0 \end{cases} \tag{3}$$

The preceding model is coupled with the conventional Euler equations through the following equations:

$$\frac{D(\rho\alpha)}{Dt} = \rho\omega_\alpha \tag{4}$$

$$\frac{D(\rho\beta)}{Dt} = \rho\omega_\beta \tag{5}$$

The governing system of equations for inviscid flows is written over an axisymmetric geometry, under ideal and adiabatic assumptions. Pressure is expressed as

$$P = (\gamma - 1)e - \rho\beta Q - 0.5\rho(u^2 + v^2) \tag{6}$$

Our experience has indicated that grid resolution is important for capturing both the wave interaction and the behavior of the reaction progress. The simplified two-step chemical reaction model does not require excessive computer time and memory, which allows us to use very fine mesh distributions. In the present work, a grid distribution of 161 × 241 for the regular regime and 161 × 301 for the large-disturbance regime are used. The finer grid distribution of 501 × 801 was also used to check the reliability of the solutions. The result showed same flow features with better resolution of wave interactions, and the reliability of the present simulations was verified.

Characteristics of Reaction

The parameters appearing in Eqs. (2) and (3) are selected as follows:

$$k_1 = 3.0 \times 10^8 \text{ m}^3/\text{kg/s}$$

$$k_2 = 2.73953 \times 10^{-5} \text{ m}^4/\text{N}^2/\text{s}$$

$$R = 397.6 \text{ J/kg/K}$$

$$E_1/R = 10,000 \text{ K}$$

$$Q = 2.2 \times 10^6 \text{ J/kg}$$

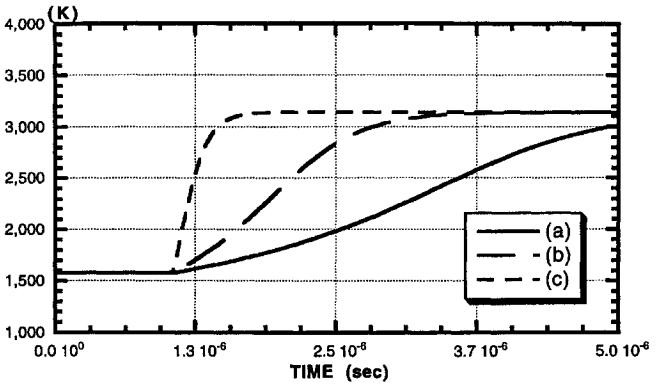

Fig. 6 Temperature profiles by the time-integration procedure in zero dimension in space under the constant volume mode of the simplified mechanism: a) $E_2/R = 5100$, b) $E_2/R = 3400$, and c) $E_2/R = 0$.

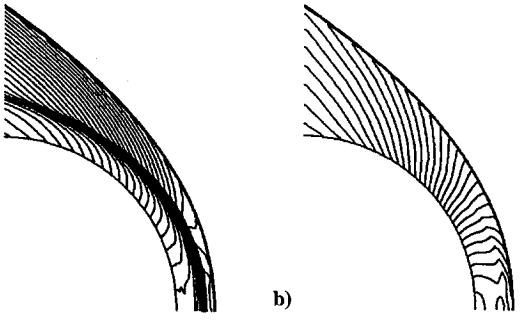

Fig. 7 Contour plots of Fig. 6a case, $E_2/R = 5100$: a) density and b) pressure.

The intensity of the concentration of heat release can be well recognized by a simple time-integration of Eqs. (2) and (3) in zero dimension in space under a constant volume mode. A computed temperature profile showing three levels of E_2/R intensity from Eq. (3) used in the present study are shown in Figs. 6a (5100), 6b (3400), and 6c (0). Here, E_2/R is used as the parameter. The method of choosing the parameter is not essential, but the temperature increasing profile is important for the flow regime.

The induction time given by the given parameters is 1.0 μs at the freestream pressure of 0.421 atm, temperature of 293 K, and projectile velocity of 1931 m/s, which corresponds to the experimental conditions of Lehr.[5]

The present work focuses on a qualitative discussion of the flowfield for the large-disturbance regime by a parametric study with the simplified chemical reaction model. Therefore, the chemistry parameters for the simplified reaction model are artificially selected to reproduce the test gas condition.

Parametric Study

Using the three values of E_2/R that correspond to the three types of heat release shown in Fig. 6, axisymmetric flow computations are carried out. Observed flow features are summarized as follows.

Figures 7a and 7b show the density and pressure contour plots for the case of low concentration of heat release (Fig. 6a case). The histories (x–t diagram) of the density and pressure level plots on the stagnation streamline are shown in Figs. 8a and 8b. Wave interactions between the bow shock and the reaction front are observed, but the compression waves are not strong enough to create the periodic unsteadiness that is usually observed as a corrugated pattern on the reaction boundary.

In the higher concentration of heat release case (Fig. 6b), the results show high-frequency and low-amplitude periodic unsteadiness that belongs to the regular regime, as observed in the density and pressure contour plots in Figs. 9a and 9b. This type of unsteadiness has been already investigated in previous work[9] using the full chemistry of 19 elementary reactions. Figures 10a and 10b show the histories (x–t diagram) of the density and pressure level plots on the stagnation streamline. The unsteadiness is periodic, and the mechanism of the wave interactions agrees with the x–t diagram

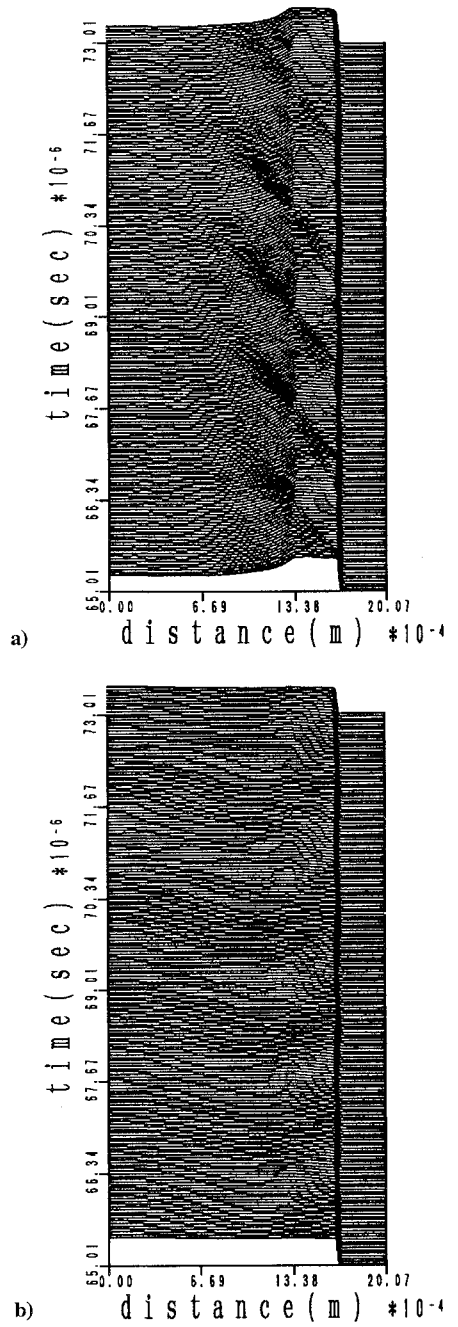

Fig. 8 Histories of level plots at each time on the stagnation streamline of Fig. 6a case, $E_2/R = 5100$: a) density and b) pressure.

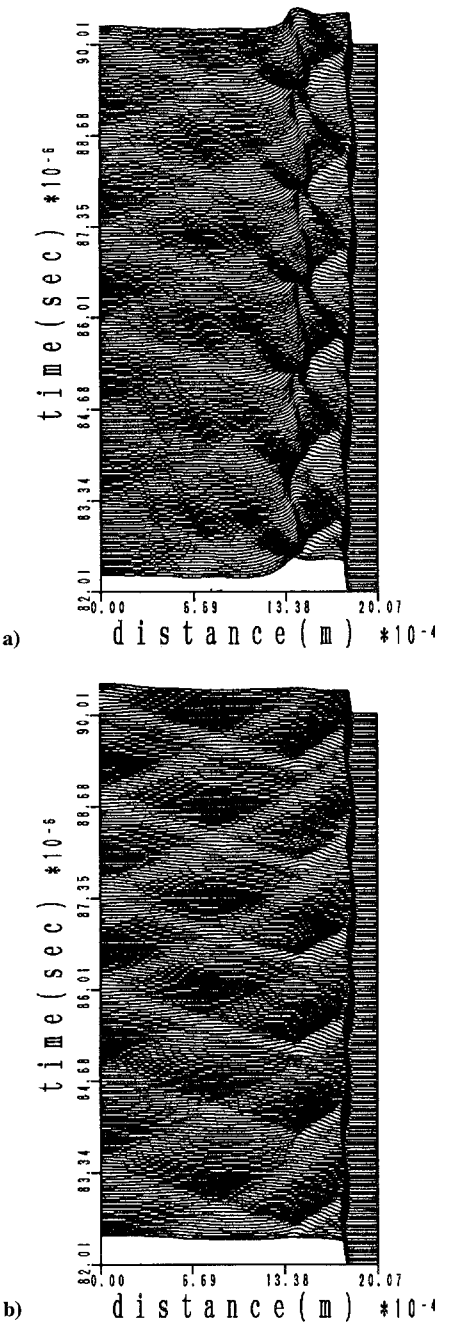

Fig. 10 Histories of level plots at each time on the stagnation streamline of Fig. 6b case, $E_2/R = 3400$: a) density and b) pressure.

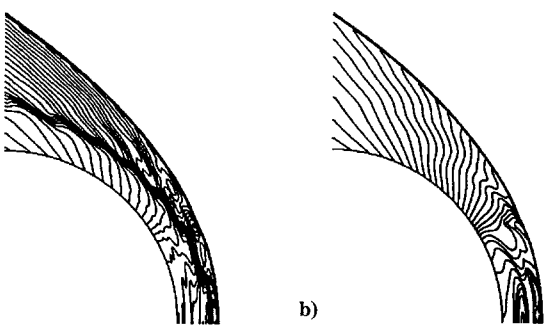

Fig. 9 Contour plots of Fig. 6b case, $E_2/R = 3400$: a) density and b) pressure.

of the one-dimensional wave interaction model in Fig. 2. This is a typical example of the wave interaction in the regular regime.

In the still higher concentration of heat release case (Fig. 6c), the result shows very unsteady structure of the combustion front. The strong wave interactions behind the bow shock are observed, and the shape of the bow shock is distorted as is observed in Figs. 11a and 11b. Figures 12a and 12b show the histories (x–t diagram) of the density and pressure level plots on the stagnation streamline.

The time histories of the pressure behind the shock wave, the so-called shock pressure, of the three cases are shown in Fig. 13. The results for the first two cases are shown in the top figure, and the third case is shown in the bottom figure, because a different pressure scale is necessary. In the Fig. 13a case, nearly periodic oscillation is seen, but the amplitude is very low and the pressure range is about 10% of the steady pressure level. In the Fig. 13b case, regularly periodic oscillation with the constant pressure range of about 30% of the steady pressure level is observed. In the Fig. 13c case, the result shows quite different behavior. Peaks of shock pressure are about double value of the steady case, and the period of the oscillation is much longer than those in Figs. 13a and 13b. Figure 13 suggests

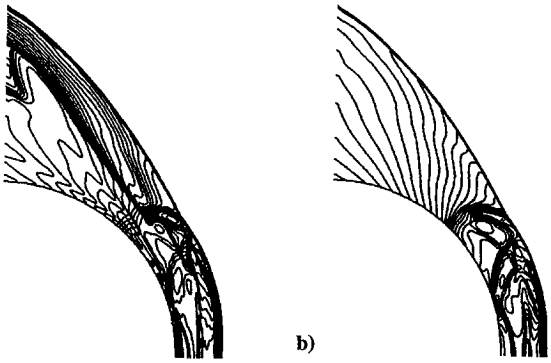

Fig. 11 Contour plots of Fig. 6c case, $E_2/R = 0$: a) density and b) pressure.

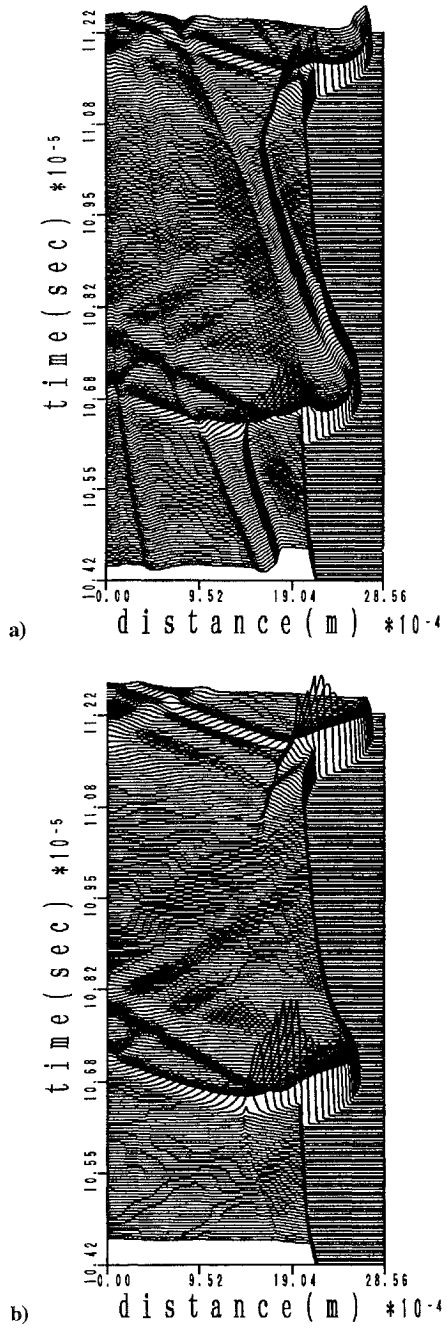

Fig. 12 Histories of level plots at each time on the stagnation streamline of Fig. 6c case, $E_2/R = 0$: a) density and b) pressure.

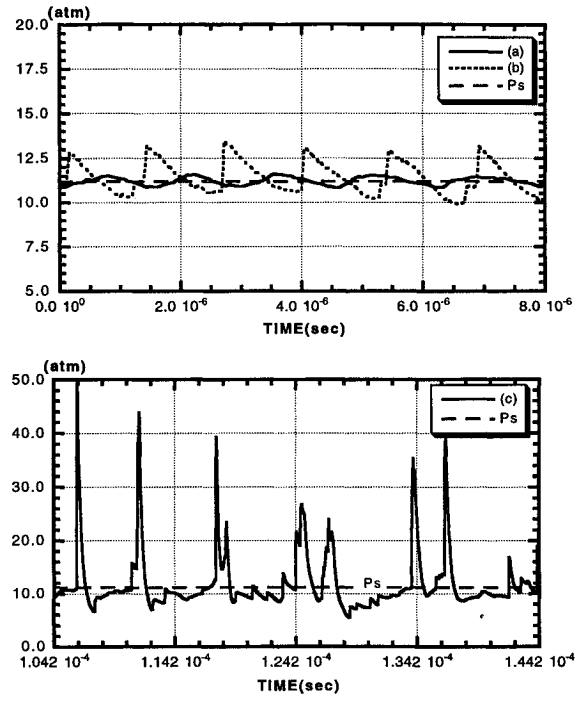

Fig. 13 History of the pressure behind the bow shock where P_s denotes the pressure level behind the steady bow shock, $P_s = 11.198$ atm: a) $E_2/R = 5100$, b) $E_2/R = 3400$, and c) $E_2/R = 0$.

that the concentration of heat release changes the structure of the shock-induced combustion around the blunt body.

Characteristics of the Stagnation Profile

The wave interactions in the third case showed a completely different structure from that of the regular regime shown in Fig. 2, and the regularly corrugated reaction boundary disappeared in Fig. 11. The oscillation became much more pronounced; lower frequency and higher amplitude of the large-disturbance regime appeared. In addition, the period of the oscillation becomes about five times longer than these of the first two cases. The period of oscillations is

$$\tau/\tau_s \approx 8$$

The period roughly agrees with the experimental results. It is evidence of the reproduction of the large-disturbance regime. The key parameters to determine the frequency of the unsteadiness are not only the induction time or length estimated by the projectile velocity. In other words, the large-disturbance regime cannot be explained by the mechanism in Fig. 2. The mechanism of the large-disturbance regime is also dominated by the wave interactions, but the roles of waves and interactions change from those of the regular regime. In the mechanism of the regular regime, the reaction shock goes to the bow shock and interacts with the bow shock, then the contact discontinuity is generated. The hotter gas behind the contact discontinuity begins to react before the contact discontinuity reaches the original reaction front, and creates a new reaction front. The most important point of the mechanism of the regular regime is the difference of the induction time before and behind the contact discontinuity. On the other hand, in the highest concentration of heat release case, an extremely strong energy release occurs on the reaction front which causes the strong reaction shock toward the bow shock and the projectile surface. The reaction shock is so strong that the gas behind the reaction shock is highly compressed, and the exothermic reaction follows and accelerates the reaction shock. The phenomenon is considered to be onset of the explosion in an explosion, producing two strong shock waves in opposite directions. The forward shock is referred to as superdetonation and moves into the unburned gas. In the opposite direction, the shock moves into the burned gas, which is known as retonation. The mechanism is usually observed as a typical example of deflagration-to-detonation transition (DDT) and has been reported in the excellent review by Oppenheim et al.[17]

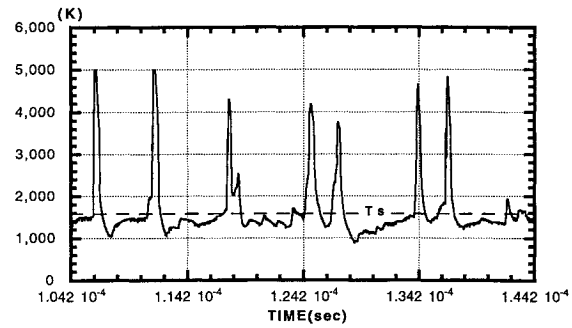

Fig. 14 History of the temperature behind the bow shock, $E_2/R = 0$. T_s denotes the temperature level behind the steady bow shock, T_s = 1576.5 K.

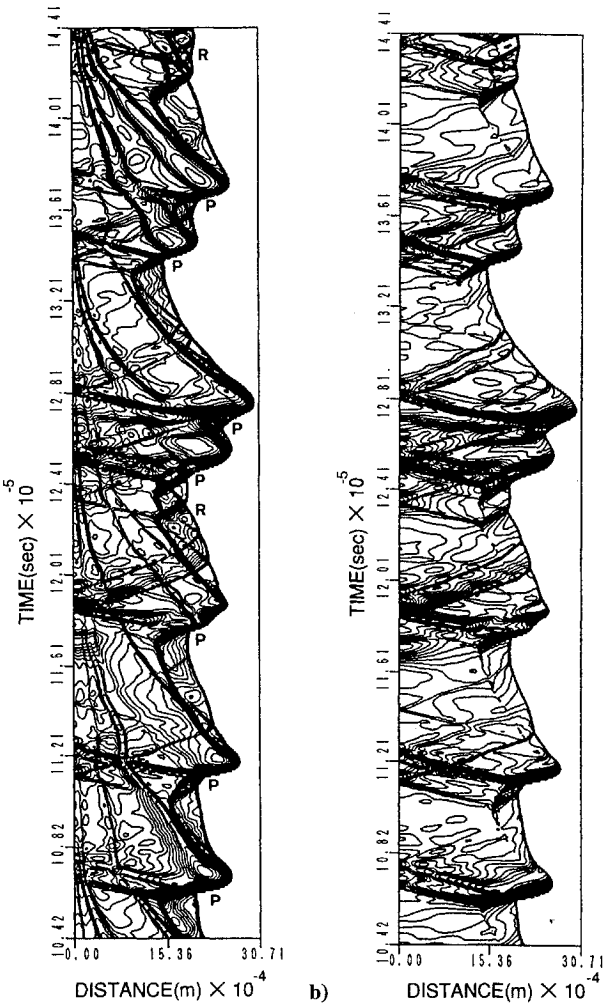

Fig. 15 Contour plots of the long series of the wave interaction of the large-disturbance regime on the stagnation streamline: a) denstiy and b) pressure. R: mechanism of the regular regime; P: penetration of the detonation wave.

The detonation wave in the unburned gas behind the bow shock overtakes and penetrates the bow shock. After the penetration, the bow shock still moves upstream, and the shock strength becomes stronger. The rarefaction wave and contact discontinuity are generated at the penetrating points. The bow shock wave accelerated by the penetration of the detonation wave is eventually decelerated, and the transition from the detonation to the shock-deflagration system, which is the ordinary shock-induced combustion, appears. When the bow shock is accelerated and moves upstream, the unburned gas is compressed more than the steady bow shock and the flowfield behind the upstream-moving shock behaves as if the projectile velocity were faster. When the bow shock is decelerated and moves downstream, the flowfield behaves as if the projectile velocity were slower.

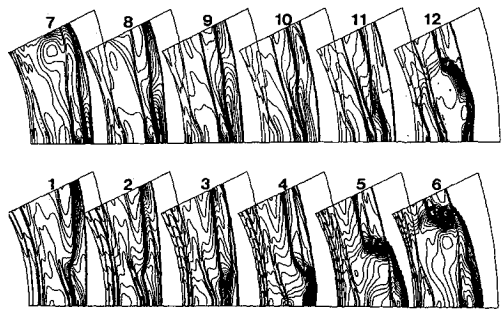

Fig. 16 Time evolution of the density contour plots in front of the projectile body, $E_2/R = 0$.

The gas temperature behind the decelerating bow shock is lower than that of the steady bow shock, so that the induction time become exponentially longer, as is seen in Fig. 12. The temperature behind the steady bow shock is 1576.5 K, but the temperature behind the decelerated bow shock is less than 1400.0 K, as is shown by the history of the temperature behind the bow shock shown in Fig. 14. Therefore, the period of oscillation becomes about five times longer than the regular regime case, as observed in the experiments.

Figures 15a and 15b show the wave interaction of the large-disturbance regime. During the interaction process, the mechanism of the regular regime is also observed, as is indicated by the R. Actually, this type of wave interaction is essentially nonlinear so that the interactions of waves and shocks are not completely periodic. However, penetrations of the detonation wave intermittently appear (see point P). Comparing the contour plots along the stagnation streamlines in Figs. 15 with the history of the shock pressure in Fig. 13c, it is recognized that penetration of the detonation wave corresponds to the peak of the shock pressure. In addition, the lower temperature periods in Fig. 14 completely agree with the decelerated bow shock in Figs. 15.

Flowfield in Front of the Projectile

Figures 16 shows the time evolution of the density contour plots in front of the projectile body. The history of the flowfield in front of the projectile body shows a feature different from that of the regular regime, and the interaction of the bow shock and the reaction front looks like the structure of the detonation wave. On the reaction front, a strong reaction shock by an explosion in an explosion is generated. The wave front overtakes and penetrates the bow shock. Finally, the triple point expands away from the axis of the projectile, and the bow shock is decelerated. Then the bow shock and the reaction front decoupled with a longer induction length than that estimated by the projectile velocity.

Model of the Large-Disturbance Regime

Figure 17 is a newly proposed one-dimensional model of the large-disturbance regime on the stagnation streamline. Basically, the mechanism is considered to be similar to the explosion in an explosion in DDT. The underdeveloped self-sustained detonation wave in front of the projectile body repeats the process under the flowfield supported by the hemispherical projectile body. The mechanism of the regular regime is also partly observed during the wave interaction, and it has a role of an initiator for the explosions on the reaction front. The reaction process of the large-disturbance regime, however, is different from the case of the regular regime, and the reaction shocks are much stronger because of the higher concentration of heat release.

The steps to be referred in the following are indicated by the bracketed numbers in the left-hand margin of Fig. 17. The beginning of the cycle is shown at step 1, when an explosion in an explosion occurs on the reaction front, and then the reaction shocks propagate upstream and downstream. The forward shock referred to as superdetonation moves into the unburned gas, and the backward shock referred to retonation moves into the burned gas. The superdetonation speed is much faster than the retonation speed due to the acceleration by the following reaction front. At step 2, the detonation wave overtakes and penetrates the bow shock. At the penetrating point, both

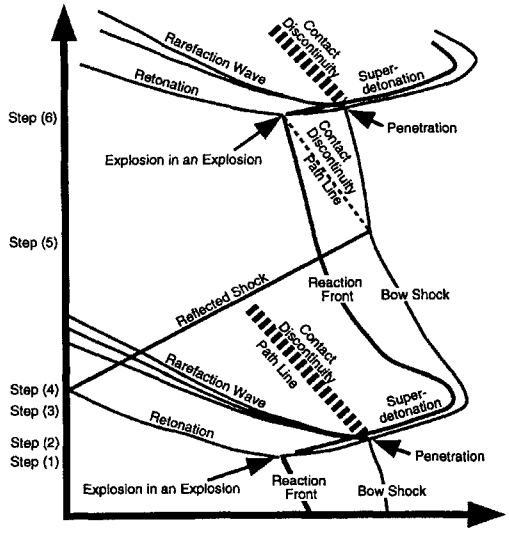

Fig. 17 Schematic picture showing the mechanism of the large-disturbance regime.

the rarefaction wave and the contact discontinuity are generated. The bow shock accelerates upstream after penetration, and the gas behind the bow shock is much compressed. At step 3, the bow shock decelerates downstream, and the separation of the bow shock and the reaction front begins. At step 4, the retonation wave reaches the body surface, and the reflected compression waves moves to the bow shock. The reflected compression wave interacts with the bow shock at step 5, and the contact discontinuity is created. The temperature behind the contact discontinuity is higher than that in front of it, so that the induction time becomes shorter. This wave interaction is the mechanism of the regular regime. Here, the induction time is much longer than that of the regular regime because the temperature behind the decelerating bow shock is much lower. At step 6, the contact discontinuity reaches the original reaction front, and the explosion in an explosion occurs on it. The cycle of events is completed as the second explosion in an explosion.

In the present simulation, the strength of the reaction shocks and the propagation of the waves are not completely the same in the cycles. As seen in Fig. 16, the flowfield around the projectile body shows the multidimensional wave propagations. The detonation wave front propagates downstream, but after propagation the bow shock separates from the reaction front. The cycle of the coupling of the bow shock and reaction front corresponds to the pulsation of the bow shock so that the bow shock wave is strongly distorted in the large-disturbance regime. It is difficult to explain the mechanism using the wave interaction on the stagnation streamline. Though the generalized one-dimensional model of the large-disturbance regime proposed in the present study explains the phenomenon well, the multidimensional flow structure may not be negligible for the flow structure of the large-disturbance regime.

Conclusions

Unsteady supersonic combustion around spherical projectiles was numerically studied using a simplified two-step chemical reaction model. Changing the intensity of the concentration of heat release, the computed flowfield showed various aspects of combustion. The simulated results revealed that the intensity of the concentration of heat release, as a key parameter, determines the regime of the unsteady flowfield observed in the experiments. The regular and large-disturbance regimes of the flowfields were reproduced in the numerical simulations, and the mechanism of the large-disturbance regime was clarified. The computed period of the peak shock pressure agreed with the experimental data, which is the evidence of reproduction of the large-disturbance regime in the present simulations. By the detailed examination of the time evolution of the wave interactions of the large-disturbance regime, a one-dimensional model explaining the mechanism of large-disturbance regime was newly proposed.

Acknowledgment

This research was supported in part by the scientific research fund from the Ministry of Education given to the first author.

References

[1]Ruegg, F. W., and Dorsey, W., "A Missile Technique for the Study of Detonation Wave," *Journal of Research of the National Bureau of Standards*, Vol. 66C, No. 1, 1962, pp. 51–58.

[2]Alpert, R. L., and Toong, T. Y., "Periodicity in Exothermic Hypersonic Flow about Blunt Projectiles," *Astronautica Acta*, Vol. 17, 1972, pp. 539–560.

[3]McVey, J. B., and Toong, T. Y., "Mechanism of Instabilities of Exothermic Hypersonic Blunt-Body Flow," *Combustion Science and Technology*, Vol. 3, 1971, pp. 63–76.

[4]Behrens, H., Struth, W., and Wecken, F., "Studies of Hypervelocity Firings into Mixtures of Hydrogen with Air or with Oxygen," *Tenth Symposium (International) on Combustion*, Combustion Inst., Pittsburgh, PA, 1965, pp. 245–252.

[5]Lehr, H. F., "Experiments on Shock-Induced Combustion," *Astronautica Acta*, Vol. 17, 1972, pp. 589–597.

[6]Abouseif, G. E., and Toong, T. Y., "Theory of Unstable One-Dimensional Detonation," *Combustion and Flame*, Vol. 45, 1982, pp. 67–94.

[7]Matsuo, A., and Fujiwara, T., "Numerical Simulation of Shock-Induced Combustion Around an Axisymmetric Blunt Body," AIAA Paper 91-1414, Jan. 1991.

[8]Matsuo, A., and Fujiwara, T., "Numerical Investigation of Oscillatory Instability in Shock-Induced Combustion Around a Blunt Body," *AIAA Journal*, Vol. 31, 1993, pp. 1835–1841.

[9]Matsuo, A., Fujii, K., and Fujiwara, T., "Flow Features of Shock-Induced Combustion Around Projectile Travelling at Hypervelocities," *AIAA Journal*, Vol. 33, 1995, pp. 1056–1063.

[10]Sussman, M. A., "Source Term Evaluation for Combustion Modeling," AIAA Paper 93-0239, Jan. 1993.

[11]Wilson, G. J., and Sussman, M. A., "Computation of Unsteady Shock-Induced Combustion Using Logarithmic Species Conservation Equations," *AIAA Journal*, Vol. 31, 1993, pp. 294–301.

[12]Ahuja, J. K., Tiwari, S. N., and Singh, D. J., "Investigation of Hypersonic Shock-Induced Combustion in a Hydrogen-Air System," AIAA Paper 92-0339, Jan. 1992.

[13]Ahuja, J. K., and Tiwari, S. N., "Numerical Simulation of Shock-Induced Combustion in a Superdetonative Hydrogen-Air System," AIAA Paper 93-0242, Jan. 1993.

[14]Korobeinikov, V. P., Levin, V. A., Markov, V. V., and Chernyi, G. G., "Propagation of Blast Waves in a Combustible Gas," *Astronautica Acta*, Vol. 17, 1972, pp. 529–537.

[15]Jachimowski, H. C., "An Analytical Study of the Hydrogen-Air Reaction Mechanism with Application to Scramjet Combustion," NASA TM-2791, Feb. 1988.

[16]Yee, H. C., "Upwind and Symmetric Shock Capturing Schemes," NASA TM-89464, 1987.

[17]Oppenheim, A. K., Manson, N., and Wagner, H. G., "Recent Progress in Detonation Research," *AIAA Journal*, Vol. 1, 1963, pp. 2243–2252.